Non-isothermal crystallization kinetics and microstructure evolution of calcium lanthanum metaborate glass

Kaushik Biswas[a], Atul D. Sontakke[a], M. Majumder[b] and K. Annapurna[a,*]
[a]Glass Technology Laboratory, [b]Instrumentation Section
Central Glass and Ceramic Research institute (CSIR)
196, Raja S. C. Mullick Road, Kolkata – 700 032, India

Abstract:

The present paper reports results on the crystallization kinetics of $35.5CaO\text{-}7.25La_2O_3\text{-}57.25B_2O_3$ glass under non-isothermal conditions based on the studies carried out from the differential thermal analysis upon using various well-established models. The crystalline phases formed during the optimized ceramization process have been confirmed from the X-ray diffraction. The activation energies of the first (formation of $CaLaB_7O_{13}$) and second (formation of $LaBO_3$) crystallization events have been estimated using the conventional methods of Kissinger, Augis-Bennett, Ozawa and Matusita and the results are found to be in good agreement with each other. The Avrami exponents that are determined by these models for the crystallization of $CaLaB_7O_{13}$ and $LaBO_3$ are found to be in the range of (1.81-2.35) and (4.03-4.65) respectively. This indicates that the formation of $CaLaB_7O_{13}$ is dominated by a surface crystallization, whereas $LaBO_3$ is formed by three-dimensional bulk crystallization with an increased rate of nucleation. This observation is further validated by microstructural investigation, which shows the formation of $CaLaB_7O_{13}$ phase as a surface layer and a bulk crystallization of $LaBO_3$ in optimally ceramized samples.

Keywords : Crystallization kinetics, differential thermal analysis, calcium lanthanum metaborate glass, glass-ceramic, activation energy

PACS : 82.20.Pm; 65.60. +a; 64.70 dg

* Corresponding author : Tel.: +91-33 2473 3469; Fax: +91-33 2473 0957
Email : glasslab42@hotmail.com (K. Annapurna)

1. Introduction

Lanthanum borate glasses have a huge potential for their use as optical components in the design of optical devices exhibiting a unique combination of optical properties like high refractive index and a relatively low mean dispersion [1-2]. However, they are fragile in nature thus lacking good glass forming ability. The addition of alkaline earth elements in this glass system improves its glass forming ability and chemical durability [1]. In addition, the alkaline earth lanthanum borate glass system exhibits a low dispersion, a high glass transition temperature and a low thermal conductivity over lanthanum borate glass system. These glasses exhibit high nonlinear optical properties with a considerably large third order nonlinear susceptibility and fast response times which enable these glasses to be greatly useful in ultra-fast all optical switching devices in the field of optical communications [3]. The glass-ceramics based on alkaline earth lanthanum borate glass system consisting of ferroelectric or nonlinear optical (NLO) crystallites have potential applications such as second harmonic generation (SHG) and nonlinear optical applications [3]. These glasses also possess low electrical conductivities and gas diffusivities hence making them attractive for high temperature hermetic sealing applications [4]. Though there have been a number of reports on the structural, optical and spectroscopic properties of this glass system, there is no report on their detailed crystallization kinetics. The crystallization kinetics of this glass system is very important to understand the formation of various crystalline phases possessing nonlinear optical property and the atomic processes involved in the formation of crystalline phases.

In this work, it has been aimed to study the crystallization kinetics of calcium lanthanum metaborate glass system. Differential thermal analysis and differential scanning calorimetry are frequently used to study the crystallization kinetics of the glassy materials [5-7]. The differential thermal analysis has been employed for such an investigation under non-isothermal conditions. The obtained data have been analyzed using well-established theoretical models like the Kissinger model [8], the Augis-Bennett model [9], the Ozawa model [10], and the Matusita model [11], and correlated with the microstructural development during crystallization.

2. Experimental

Calcium lanthanum metaborate glass with composition of 35.5 CaO-7.25 La_2O_3-57.25 B_2O_3 in atomic fraction was prepared using the high purity (99.99%) raw chemicals such as H_3BO_3, $CaCO_3$, and La_2O_3 in pure platinum crucible at 1573 K temperature by adopting

conventional melt quench technique followed by annealing at 923 K for 1 h. Subsequently, the annealed glass samples were cut to the desired sizes and were then processed for carrying out further experiments. The samples were ceramized at three different temperatures of 1013, 1043, and 1083 K for 30 min. The amorphous nature of the prepared glasses was verified and phase identification of the heat-treated samples was carried out on an X-ray diffractometry (XRD) on X'Pert, PANalytical using Ni-filtered CuK_{α} radiation with wavelength of 1.5406 Å. The differential thermal analysis (DTA) of all glasses was performed in air atmosphere using platinum crucible with an empty one as a reference in the temperature range of room temperature to 1250 K on Netzsch differential thermal analyzer model STA 409 at different heating rates of 10, 20, 30, 40 K min^{-1} to obtain various thermal data after the baseline correction by subtracting the baseline from the initial run. The microstructural investigation was carried out by Field emission scanning electron microscopy (FE-SEM) on Supra 35 VP of Carl Zeiss for the differently ceramized samples.

3. Results and Discussion

3.1. Thermal stability and XRD analysis:

The DTA curves of calcium lanthanum metaborate glass at different heating rates of 10, 20, 30 and 40 K min^{-1} are depicted Fig. 1. All these DTA curves show distinct T_g followed by two crystallization peaks (T_{p1} and T_{p2}). The crystallization onset (T_x) temperatures are estimated from the intersections of the slopes to the curves at endothermic and first exothermic peaks. From the data determined from differential thermal analysis, the glass stability factor ($\Delta T = [T_x - T_g]$) was estimated. The thermal data calculated at different heating rates are summarized in Table 1 along with their respective error bars. A weak exothermic signal is observed in between T_g and T_x for all the measurements at various heating rates. This signal could originate due to the structural relaxation, which masks the glass-liquid transition and is a characteristic of an amorphous solid.

Fig. 2 (a) shows the XRD pattern of the calcium lanthanum metaborate glasses. The diffraction pattern of the as-quenched glass consists of a broad maximum with no appreciable diffraction peaks corresponding to crystalline phases indicating its amorphous structure. For optimized ceramization, three different temperatures of 1013 K (before the first crystallization peak temperature), 1043 K (near the first crystallization peak temperature), and 1083 K (near the second crystallization peak temperature) were selected from the DTA curve obtained with heating rate of 10 K min^{-1}. XRD patterns of the specimens ceramized at these temperatures for 30 min are shown in Fig. 2 (b), (c), and (d), respectively. Analysis of

the XRD pattern reveals that crystallization hardly occurs in the sample ceramized at 1013 K. The samples ceramized at 1043 K shows the presence of only one crystalline phase, $CaLaB_7O_{13}$ (JCPDS No 44-0353) with monoclinic structure, while the sample ceramized at 1083 K shows the presence of $CaLaB_7O_{13}$ and $LaBO_3$ (JCPDS No. 12-0762) with orthorhombic crystal structure. The XRD peaks have been appropriately assigned for the respective crystalline phases in Fig. 2.

3.2. The kinetics of crystallization:

To evaluate the effective energy barrier for non-isothermal crystallization process for the crystallization of $CaLaB_7O_{13}$ and $LaBO_3$, several models like Kissinger method [8], Augis and Bennett method [9], Ozawa method [10], and Matusita method [11] were adopted. Kissinger equation is the most commonly used model in analyzing the activation energy of both crystallization event (E_c) and glass transition (E_g). This model describes the dependence of peak temperature on heating rate for a crystallization event. To estimate the activation energies for crystallization, this method has been applied for the analysis of both the exothermic peaks (T_{p1} and T_{p2}) detected in DTA curves using the following equation [8]:

$$\ln\frac{\beta}{T_p^2} = -\frac{E_c}{RT_p} + \text{const.}, \quad \ldots\ldots\ldots\ldots\ldots\ldots\ldots\ldots(1)$$

Fig. 3 shows the plot of ($\ln \beta/T^2_p$) versus ($1000/T_p$) for all heating rates for the two crystallization events along with their straight regression lines derived by least squares fitting with correlation coefficients (R). From the slopes of the straight lines, the activation energies have been evaluated to be 531.3 kJ mol^{-1} and 173.3 kJ mol^{-1} for the first and second crystallization peaks, respectively.

The activation energies of the crystallization events can also be determined by an approximation method developed by Augis and Bennett [9]. Their approach showed a linear relation between ($\ln \beta/T_p$) and ($1/T_p$) in contrast to the linear relation between ($\ln \beta/T^2_p$) and ($1/T_p$) as described by Kissinger model. Hence, this method is based on the following equation [9]:

$$\ln\frac{\beta}{T_p} = -\frac{E_c}{RT_p} + \text{const.} \ldots\ldots\ldots\ldots(2)$$

The plot between $\ln (\beta/T_p)$ vs ($10^3/T_p$) is presented in Fig. 4 together with their straight regression lines and correlation coefficients. The activation energies calculated from the slopes are 535.8 kJ mol^{-1} and 175.7 kJ mol^{-1} for the first and second crystallization peaks,

respectively. Furthermore, using the value of activation energy for each crystallization event, the Avrami exponent can be calculated using the following equation [9]:

$$n = \frac{2.5RT_p^2}{\Delta T_{FWHM} E_c}, \ldots\ldots\ldots\ldots (3)$$

where, ΔT_{FWHM} is the full width of the exothermic peak at the half maximum intensity. Thus, ΔT_{FWHM} was estimated at various heating rates for the two crystallization peaks and the evaluated Avrami exponents (n) for the two crystallization peaks are listed in Table 2. The average Avrami exponent calculated for the first crystallization event and second crystallization events are 1.81 and 4.03, respectively.

Another widely used non-isothermal method to determine the activation energy is the Ozawa model [10], which considers that the transformation under non-isothermal condition is represented by a first-order reaction, and this is also the case with the Kissinger model. The model proposed by Ozawa showed a linear relation between (ln β) *and* ($1/T_p$), whereas Kissinger model considered the linear relation between (ln β/T_p^2) and ($1/T_p$). The Ozawa model is described as [10]:

$$\ln \beta = -\frac{E_c}{RT_p} + \text{const.}, \ldots\ldots\ldots\ldots (4)$$

The plot of ln (β) versus ($1000/T_p$) and their straight regression lines are shown in Fig. 5. From the slope of the line, the activation energy was calculated for each crystallization event. The activation energy determined following this model was 544.5 kJ mol^{-1} and 185.1 kJ mol^{-1} for the first and second crystallization peaks, respectively.

Matusita has developed a model to calculate the activation energy during non-isothermal crystallization considering the concept of nucleation and growth [11]. According to this model, crystallization mechanisms (e.g bulk or surface crystallization) should be taken into consideration to estimate the activation energy. Unlike Kissinger and Ozawa models, Matusita model provides information about the Avrami exponent and dimensionality of growth. It was proposed that the volume fraction of crystallites, x, precipitated in a glass heated at constant rate, β, is related to the crystallization activation energy, E_c, through the following expression [11]:

$$\ln[-\ln(1-x)] = -n \ln \beta - 1.052 \frac{mE_c}{RT} + \text{const.}, \ldots\ldots\ldots\ldots (5)$$

where, m and n are integers or half-integers and m is the is the dimensionality of growth and n is the Avrami exponent. Fig. 6 (a) and (b) show the relationship between the crystallized volume fraction (x) and temperature for the first and second crystallization events at different heating rates, respectively, displaying typical sigmoidal-type curves. Crystallization fractions at different temperatures were determined from DTA thermograms (Fig. 1) on integrating the area under the exotherms and then by normalizing the cumulative area by total area under the exotherms. From Figs. 6 (a) and (b), we obtained plots of ln[-ln(1-x)] against ln β at various fixed temperatures. In this study, for the first crystallization peak, three fixed temperatures of 1033, 1038 and 1043 K were selected, whereas for the second peak, the fixed temperatures were 1113, 1118, and 1123 K at equal intervals as shown in Figs.7 (a) and (b). The linear regression lines obtained by least squares fitting are also represented in Fig. 7 (a) and (b) along with their respective correlation coefficient values at various temperatures. From the slope of these curves, the order of the Avrami index, n, could be obtained and the mean values of n were found to be 2.35 and 4.65, for the first and second crystallization peaks, respectively. Furthermore, the activation energy for crystallization (E_c), can also be calculated from Matusita equation (eqn. (5)). For as-quenched glass which is free from the presence of any nuclei, $n = m+1$, while for a glass containing sufficiently large number of nuclei, $n = m$. Hence, for the first crystallization peak, considering the fact that there is no nuclei before the formation of the crystalline phase in the as quenched glass, $m = (n-1) = 1.35$. For the second crystallization peak, as there are number of nuclei of the first crystalline product already in the glass matrix, $m = n = 4.65$. Using these values of m, the activation energy for crystallization can be calculated from the slope of the line obtained on plotting ln[-ln(1-x)] versus (1000/T) using eqn. (5) as shown in Fig 8 (a) and (b). Thus determined average activation energies for the first and second crystallization peaks are 579.6 kJ mol^{-1}, and 186.5 kJ mol^{-1}, respectively.

The activation energies of the two crystallization events calculated by means of different theoretical models as described above are summarized in Table 3 along with their respective error bars. The activation energies estimated from various models are in the same range for both the crystallization events. However, on close observation of the data, it could be noticed that there is slight increase in the crystallization activation energies determined by Matusita and Sakka's model compared to other models. This may be attributed due to the fact that the different models have adopted slightly different assumptions. For the Kissinger, Augis-Bennett and Ozawa models, the concept of nucleation and growth has not been considered. But Matusita and Sakka's model is developed on the basis that crystallization occurs by

nucleation and growth process which include several mechanisms such as bulk crystallization by two or three dimensional growth or surface crystallization governed by one or two dimensional growth. The activation energy determined by means of the above-mentioned theoretical models refers to the activation energy of the overall process which includes both nucleation and growth. Moreover, it is found that the activation energy for the first crystallization event corresponding to the formation of $CaLaB_7O_{13}$ is higher than that of the second crystallization event corresponding to the formation of $LaBO_3$. This could arise from the fact that some crystallites of $CaLaB_7O_{13}$ formed during first crystallization and their additional interfaces act as favourable nucleating sites and aid the crystallization process of $LaBO_3$ reducing the activation energy of the later. After the crystallization of $CaLaB_7O_{13}$ phase, the residual glass matrix becomes boron-deficient and hence, much prone to crystallization. This could be another reason for the reduction of activation energy for the crystallization of $LaBO_3$.

Further, in order to understand the change in activation energy with increase in crystallization fraction during the crystallization process, on the basis of the DTA curves at various heating rates, the isoconversional method of Flynn, Wall and Ozawa was used [12-14]. From this model, activation energy at a fixed crystallization fraction can be estimated measuring different temperatures at different heating rates, β according to following equation:

$$\ln\frac{\beta}{T^2} = -\frac{E_c}{RT} + \text{const.}, \ldots\ldots\ldots\ldots(6)$$

Then, from the slope of the plot between (ln β/T^2) and (1000/T), the value of activation energy is calculated at fixed crystallization volume fractions. For our study, the activation energies were calculated at crystallization volume fractions ranging from 0.05-0.95 with an interval of 0.05 for each crystallization event. Fig. 9 shows the variation of activation energy with crystallization volume fraction. For the first crystallization peak, E_c decreases from 541.8 kJ mol^{-1} to 287.3 kJ mol^{-1}, whereas, for the second crystallization peak, local activation continuously decreases from 227.5 kJ mol^{-1} to 132.7 kJ mol^{-1}. For both the cases, increased number of nucleating sites and interfaces could reduce the local activation energy thus causing a further progress in crystallization.

The kinetics for isothermal solid-state phase transformation (here glass to crystal) is described by Kolmogorov-Johnson-Mehl-Avrami (KJMA) theory [15-17], here the volume

fraction of crystallization (x) after a certain time (t) can be correlated with reaction constant (K) and Avrami exponent (n) as per the following equation:

$$x = 1 - \exp[-(Kt)^n], \ldots\ldots\ldots\ldots\ldots\ldots\ldots\ldots(7)$$

According to this theory, the value of avrami exponent (n) being close to 2 indicates that surface crystallization dominates overall crystallization, while the value of 3 implies a two dimensional and the value of 4 indicates a three dimensional crystallization for bulk materials. The parameter, n, can be written as $n=b+pm$, where p is taken as 1 for linear growth and 0.5 for parabolic growth and m is equal to 1, 2 or 3 for one-, two- or three-dimensional growth, respectively and $b = 0$ for no nucleation, $b < 1$ for decreasing nucleation and $b > 1$ for increasing nucleation rate [18]. In the present study, the Avrami exponent determined by Augis and Bennett's model for the crystallization of $CaLaB_7O_{13}$ is 1.81, whereas for the crystallization of $LaBO_3$, it is 4.03. The Avrami exponents estimated by Matusita and Sakka's model are 2.35, and 4.65 for the crystallization of $CaLaB_7O_{13}$ and $LaBO_3$, respectively. Thus, it can be inferred that the formation of $CaLaB_7O_{13}$ is dominated by two-dimensional surface crystallization [19]. In general, values of $n > 4$ are not considered in theories of phase transformation kinetics. Crystallization events, for which $3 < n < 4$, are considered to follow diffusion controlled transformation process with a nucleation rate which decreases with time. It has suggested that $n > 4$ could be obtained if the nucleation rate increases with time [20]. Thus, it can be inferred that the formation of $LaBO_3$ is dominated by three-dimensional bulk crystallization process with increasing nucleation rate.

3.3. Microstructural investigation:

The sample ceramized at 1013 K for 30 min does not show any evidence of crystallization in the microstructure and exhibited a featureless matrix. This corroborates the results of XRD (Fig 2 (b)), which showed the absence of any crystalline phases in the sample. The FESEM micrographs of samples ceramized at 1043 and 1083 K for 30 min are shown in Fig. 11. The sample ceramized at 1043 K exhibited (Fig. 10 (a)) a surface layer of thickness varying from 110-210 µm (Region S). XRD analysis confirmed this layer to be $CaLaB_7O_{13}$ (Fig. 2 (c)). However, there is no evidence of bulk crystallization in this sample and the bulk region exhibits featureless matrix (Region G1). In case of the sample ceramized at 1083 K for 30 min, the presence of crystalline phase in the bulk of the sample has been observed together with the surface layer. However, the thickness of the surface layer becomes higher when compared with the sample ceramized at 1043 K and ranges from 250-490 µm. Furthermore, it is observed that the surface layer of $CaLaB_7O_{13}$ advances towards the bulk region randomly (Fig. 10 (b)). In a very few regions near the surface, this phase is also formed as minor bulk

crystalline phase (Fig. 10 (b)) dispersed along with the major crystalline phases of $LaBO_3$ in the bulk. The Avrami exponent determined for the first crystallization was close to 2 and this indicated the formation of $CaLaB_7O_{13}$ is dominated by surface crystallization. However, it can be seen from the microstructural analysis that the formation $CaLaB_7O_{13}$ phase does not occur by purely one-dimensional growth during surface crystallization. The crystallization process began mainly from the surface with a minor fraction extending towards inside. A few crystals of $CaLaB_7O_{13}$ grew simultaneously from the inside of this glass. This also explains the reason for the deviation of the Avrami exponent value from 1, which is meant for purely one-dimensional growth for surface crystallization.

A high magnification FESEM micrograph (Fig. 10 (b)) taken from the selected bulk region of the sample shows the presence of $LaBO_3$ (region B) and residual glass (region G2) in the microstructure. It is observed that $LaBO_3$ phase is distributed in the form of clusters of tiny granules (1-3 μm) dispersed in the glassy matrix. Furthermore, the morphology of $LaBO_3$ phase ensured that the phase is formed by three dimensional bulk crystallization process. This observation is in agreement with the value of Avrami exponents as determined from Augis and Bennett's model (n = 4.03) and Matusita and Sakka's model (n = 4.65).

4. Conclusions:

In summary, it could be concluded as follows:

1. The crystallization of 35.5 CaO-7.25 La_2O_3-57.25 B_2O_3 glass took place from a two-step crystallization process. XRD analysis confirms that the first and second crystallizations are due to the formation of $CaLaB_7O_{13}$ and $LaBO_3$ phases, respectively.
2. The activation energies for the crystallization (E_c) were estimated from Kissinger, Augis and Bennett, Ozawa and Matusita methods for $CaLaB_7O_{13}$ is 531.3, 535.8, 544.5 and 579.6 kJ mol^{-1}, whereas for $LaBO_3$, is 173.3, 175.7, 185.1, and 186.5 kJ mol^{-1}, respectively. Based on the magnitudes of Avrami exponents (n), it could be inferred that two-dimensional surface crystallization would dominate the formation of $CaLaB_7O_{13}$ and three-dimensional bulk crystallization process, which govern the crystallization of $LaBO_3$.
3. FESEM micrographs indicate the formation of a surface layer of $CaLaB_7O_{13}$ from the optimally ceramized samples corroborating the phenomenon of surface crystallization. Further three dimensional growth of $LaBO_3$ phase in the form of clusters of tiny granules (1-3 μm) from the samples that were ceramized at 1083 K for 30 min was observed.

Acknowledgements:

Authors would like to express their grateful thanks to Dr. H. S. Maiti, Director, CGCRI for his kind encouragement and permission to publish this work. Our thanks are also due to Dr. Ranjan Sen, for his kind support in the present work. One of us (ADS) is thankful to the CGCRI, CSIR for the award of a Research Internship to him.

References:

1. Brow RK, Tallant DR, Turner GL. Raman and ^{11}B Nuclear Magnetic Resonance Spectroscopic Studies of Alkaline-Earth Lanthanoborate Glasses. J Am Ceram Soc. 1996; 79:2410-14.

2. Chakraborty IN, Day DE**.** Effect of R^{3+} Ions on the Structure and Properties of Lanthanum Borate Glasses. J Am Ceram Soc. 1985; 68:641-5.

3. Dyamant I, Korin E, Hormadaly J. Thermal and some physical properties of glasses in the La_2O_3-CaO-B_2O_3 ternary system. J Non-Cryst Solids. 2008; 354:3135-41.

4. Sohn SB, Choi SY, Kim GH, Song HS, Kim GD. Stable sealing glass for planar solid oxide fuel cell. J Non-Cryst Solids. 2002; 297:103-12.

5. Mehta N, Kumar A. Comparative analysis of calorimetric studies in $Se_{90}M_{10}$ (M=In, Te, Sb) chalcogenide glasses. J Therm Anal Calorim. 2007;87:345–50.

6. Sánchez-Jiménez PE, Criado JM, Pérez-Maqueda LA. Kissinger kinetic analysis of data obtained under different heating schedules. J Therm Anal Calorim. 2008;94:427–32.

7. Nitsch K, Rodová M. Crystallization study of Na–Gd phosphate glass using non-isothermal DTA. J Therm Anal Calorim.2008;91:137–40.

8. Kissinger HE. Variation of peak temperature with heating rate in differential thermal analysis. J Res Nat Bur Stand. 1956; 57:217-21.

9. Augis JA, Bennett JE. Calculation of the Avrami parameters for heterogeneous solid state reactions using a modification of the Kissinger method. J Therm Anal. 1978; 13:283-92.

10. Ozawa T. A New Method of Analyzing Thermogravimetric Data. Bull Chem Soc Jpn. 1965; 38:1881-86.

11. Matusita K, Sakka S. Kinetic study of the crystallization of glass by differential scanning calorimetry. Phys Chem Glasses. 1979; 20:81-4.

12. Flynn JH, Wall LA. General treatment of the thermogravimetry of polymers. J Res Nat Bur Stand. 1966;70A:487-523.

13. Ozawa T. Kinetic analysis of derivative curves in thermal analysis. J Therm Anal. 1970; 2:301-24.

14. Yuan ZZ, Chen XD, Wang BX, Wang YJ. Kinetics study on non-isothermal crystallization of the metallic $Co_{43}Fe_{20}Ta_{5.5}B_{31.5}$ glass. J Alloys Compd. 2006; 407:163-9.

15. Kolmogorov AN. On the statistical theory of the crystallization of metals. Bull. Acad. Sci USSR Phys Ser. 1937;3:355-9.

16. Johnson WA, Mehl RF. Reaction kinetics in processes of nucleation and growth. Trans Am Inst Met Eng. 1939;135:416-42.

17. Avrami MJ. Granulation phase change and microstructure kinetics of phase change. III. J Chem Phys. 1941;9:177–84.

18. Liu F, Yang G. Effects of anisotropic growth on the deviations from Johnson–Mehl–Avrami kinetics. Acta Mater. 2007;55:1629-39.

19. Majhi K, Varma KBR. Crystallization kinetics of $SrBi_2B_2O_7$ glasses by non-isothermal methods. J Therm Anal Calorim. 2009;doi: 10.1007/s10973-009-0105-5

20. Araújo EB, Idalgo E. Non-isothermal studies on crystallization kinetics of tellurite $20Li_2O$-$80TeO_2$ glass. J Therm Anal Calorim.2009;95:37–42.

Figure captions

Fig. 1 DTA curves of 35.5 CaO-7.25 La_2O_3-57.25 B_2O_3 glass at different heating rates

Fig. 2 X-ray diffraction patterns of (a) as-quenched of 35.5 CaO-7.25 La_2O_3-57.25 B_2O_3 glass and glasses ceramized at (b) 1013 K, (c) 1043 K, and (d) 1083 K for 30 min

Fig. 3 $\ln(\beta/T_p^2)$ versus $(1000/T_p)$ of 35.5 CaO-7.25 La_2O_3-57.25 B_2O_3 glass for 1st and 2nd crystallization peaks

Fig. 4 $\ln(\beta/T_p)$ versus $(1000/T_p)$ of 35.5 CaO-7.25 La_2O_3-57.25 B_2O_3 glass for 1st and 2nd crystallization peaks

Fig. 5 $\ln(\beta)$ versus $(1000/T_p)$ of 35.5 CaO-7.25 La_2O_3-57.25 B_2O_3 glass for 1st and 2nd crystallization peaks

Fig. 6 The crystallization fraction versus temperature of 35.5 CaO-7.25 La_2O_3-57.25 B_2O_3 glass for (a) 1st and (b) 2nd crystallization peaks at different heating rates

Fig. 7 $\ln[-\ln(1-x)]$ versus $\ln \beta$ of 35.5 CaO-7.25 La_2O_3-57.25 B_2O_3 glass for (a) 1st and (b) 2nd crystallization peaks at different heating rates

Fig. 8 $\ln[-\ln(1-x)]$ versus $(1000/T)$ of 35.5 CaO-7.25 La_2O_3-57.25 B_2O_3 glass for (a) 1st and (b) 2nd crystallization peaks at different heating rates

Fig. 9 Variation of the activation energy with the crystallization fraction of 35.5 CaO-7.25 La_2O_3-57.25 B_2O_3 glass for 1st and 2nd crystallization events

Fig. 10 FE-SEM micrographs showing the microstructure of 35.5 CaO-7.25 La_2O_3-57.25 B_2O_3 glasses ceramized at (a) 1043 K and (b) 1083 K for 30 min

Table 1: Thermal properties of 35.5 CaO-7.25 La_2O_3-57.25 B_2O_3 glass at different heating rates.

Heating rates / K min^{-1}	**Glass transition temperature (T_g)/ K**	**Crystallization onset temperatures (T_x) / K**	**Crystallization peak temperature / K**		**Glass Stability Factor ΔT / K**
			First (T_{p1})	Second (T_{p2})	
10	912 ± 3	1014 ± 2	1039 ± 1	1101 ± 1	102
20	920 ± 3	1017 ± 2	1050 ± 1	1127 ± 1	97
30	922 ± 3	1020 ± 2	1059 ± 1	1154 ± 1	98
40	924 ± 3	1024 ± 2	1061 ± 1	1181 ± 1	100

Table 2: Full width of the exothermic peak at the half maximum intensity (ΔT_{FWHM}) and Avrami exponents (n) of 35.5 CaO-7.25 La_2O_3-57.25 B_2O_3 glass.

Heating rates / K min^{-1}	**1st crystallization peak**		**2nd crystallization peak**	
	ΔT_{FWHM}/K	n	ΔT_{FWHM}/ K	n
10	19	2.20	29	4.94
20	21	2.04	33	4.55
30	28	1.55	44	3.58
40	30	1.46	54	3.05

Table 3: Values of the activation energy for crystallization (E_c) deduced from different methods for the first and second crystallization events of 35.5 CaO-7.25 La_2O_3-57.25 B_2O_3 glass.

Name of method	**E_c/ kJ mol^{-1}**	
	1st crystallization	2nd crystallization
Kissinger	531.3 ± 47	173.3 ± 25
Augis and Bennett	535.8 ± 47	175.7 ± 25
Ozawa	544.5 ± 47	185.1 ± 25
Matusita	579.6 ± 35	186.5 ± 10

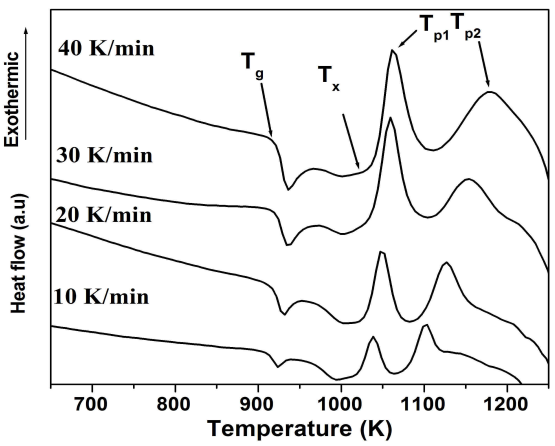

Fig. 1

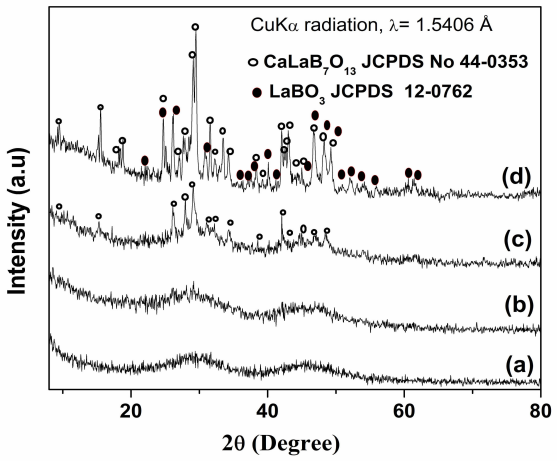

Fig. 2

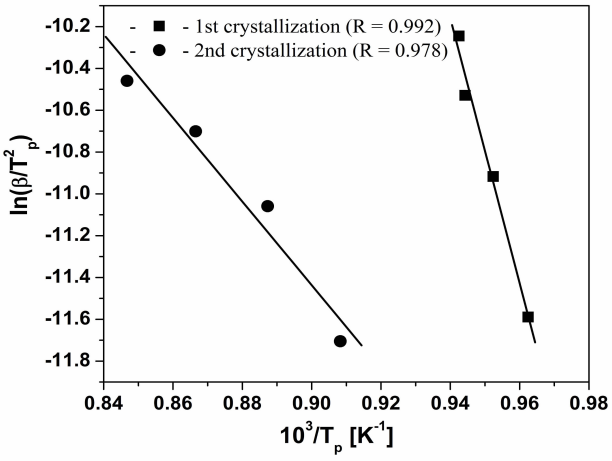

Fig. 3

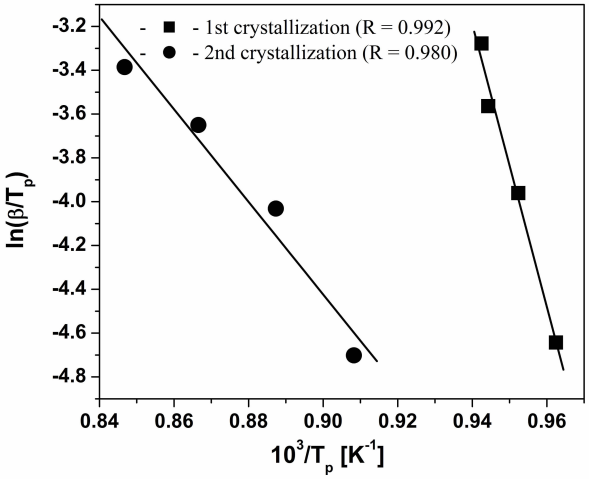

Fig. 4

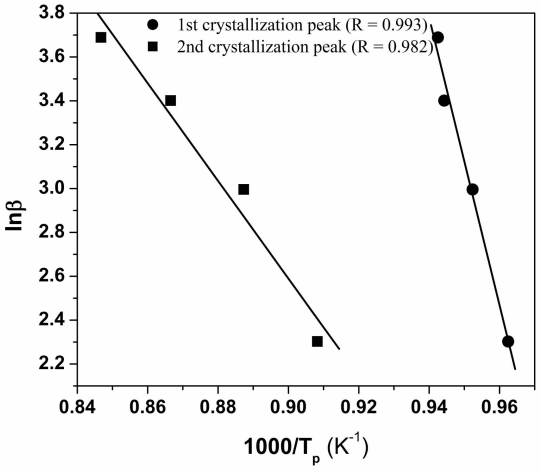

Fig. 5

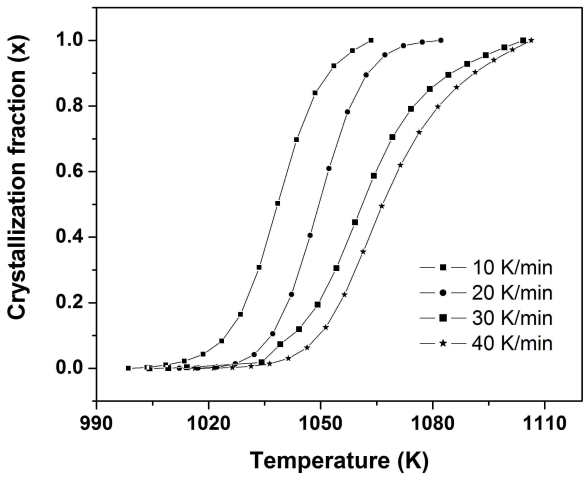

(a)

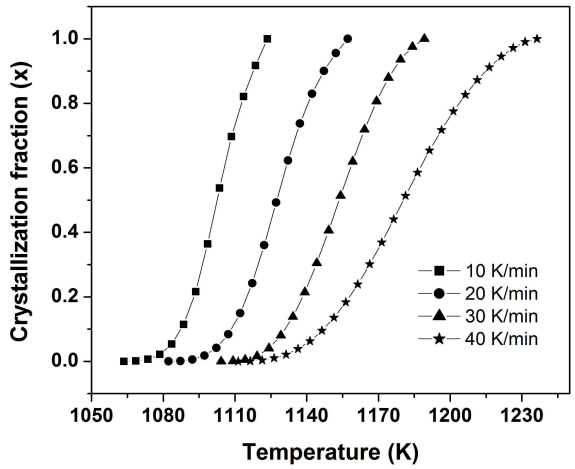

(b)

Fig. 6

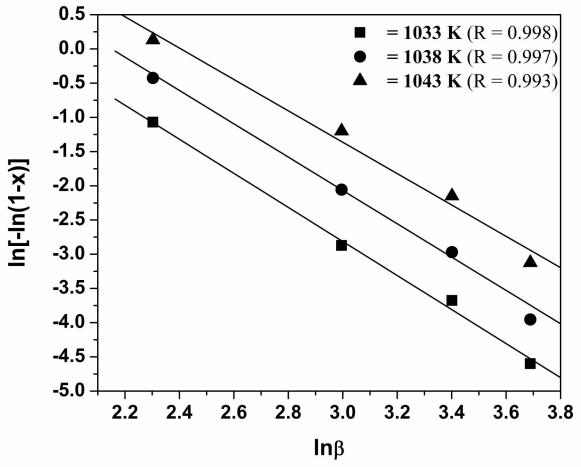

(a)

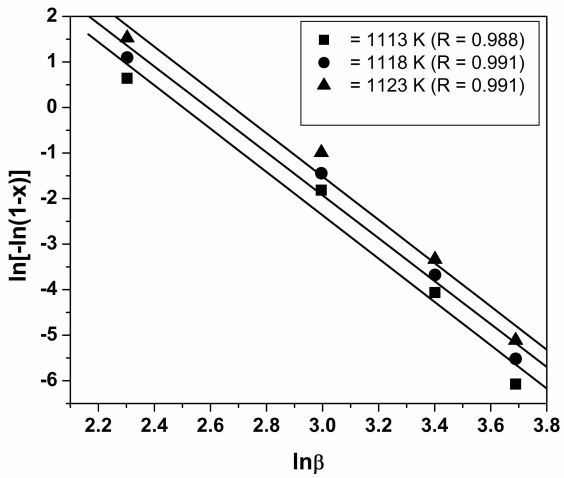

(b)

Fig. 7

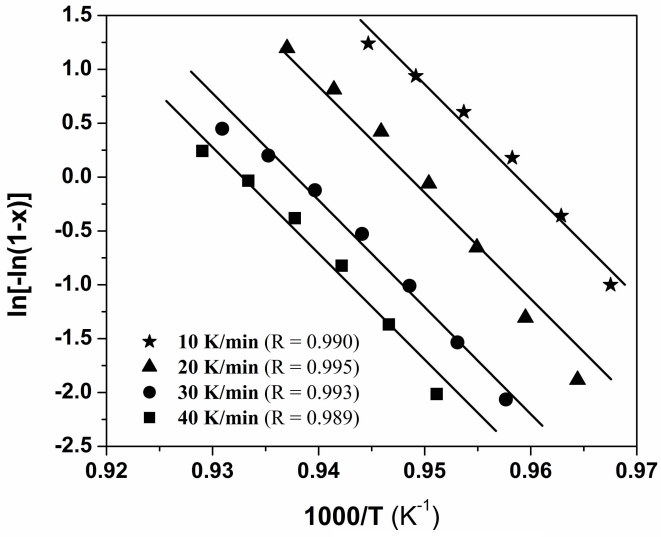

(a)

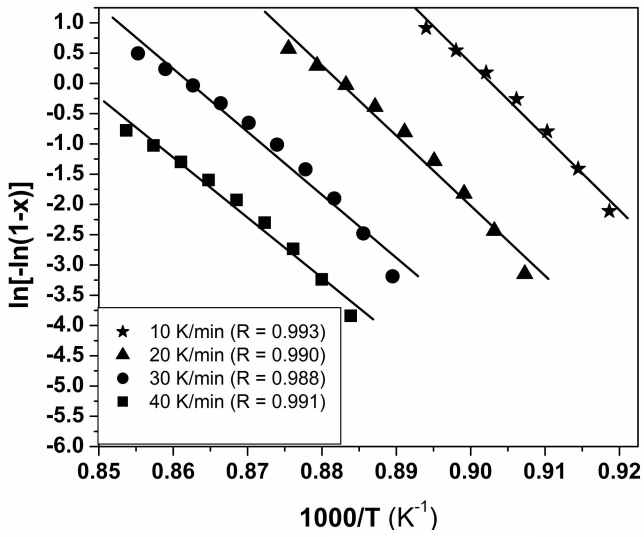

(b)

Fig. 8

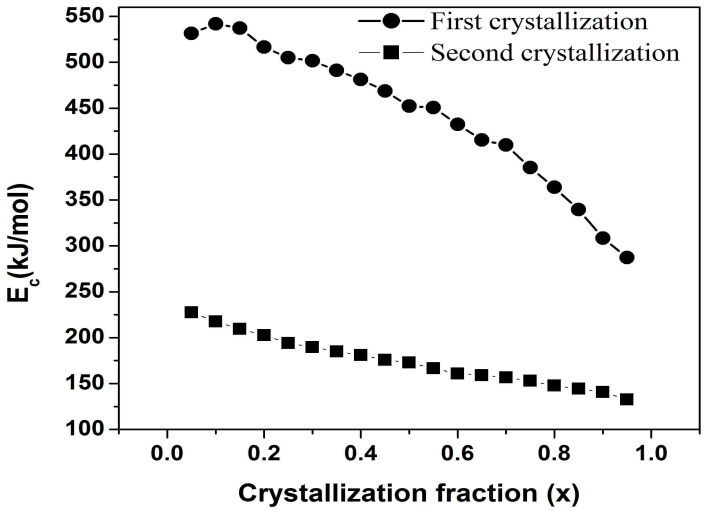

Fig. 9

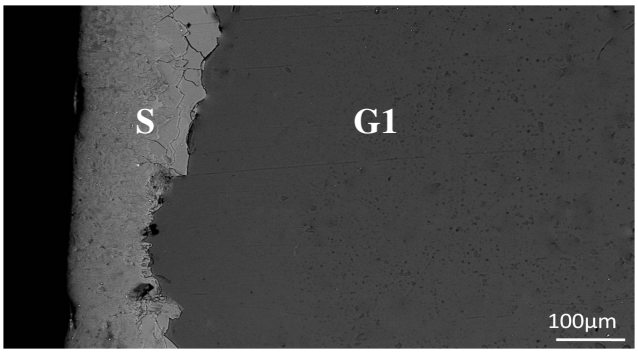

(a)

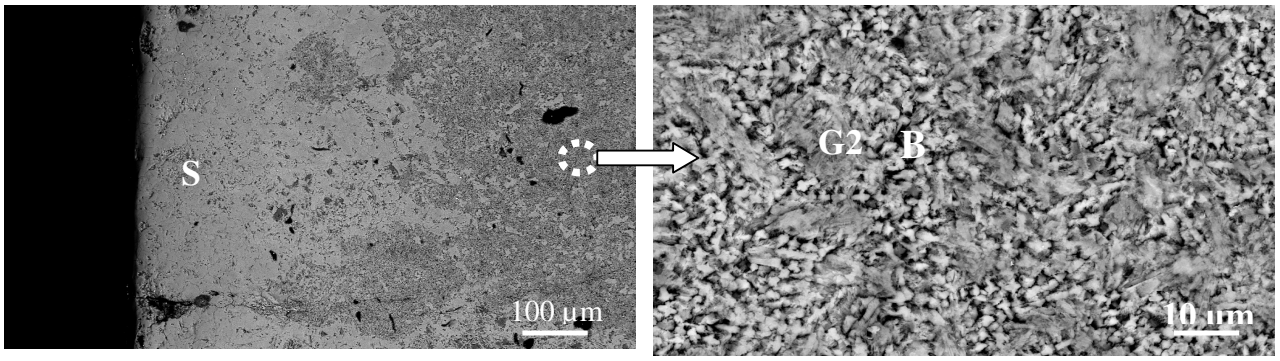

(b)

Fig. 10